Two- and three-dimensional band structure of ultrathin Ni on Cu(001)

Moritz Hoesch,[1] Vladimir N. Petrov,[2] Matthias Muntwiler,[3,*] Matthias Hengsberger,[3] Jorge Lobo Checa,[3,†] Thomas Greber,[3] and Jürg Osterwalder[3]

[1]*European Synchrotron Radiation Facility, 6 rue Jules Horowitz, 38043 Grenoble Cedex, France*

[2]*St. Petersburg State Polytechnical University, St. Petersburg 195251, Russia*

[3]*Physikinstitut der Universität Zürich, Winterthurerstrasse 190, CH-8057 Zürich, Switzerland*

(Received 31 October 2008; revised manuscript received 25 February 2009; published 2 April 2009)

The momentum-resolved electronic structure of ultrathin films of Ni on Cu(001) is investigated by angle-resolved photoemission in the thickness range between 2 and 6 monolayers and by first-principles slab calculations. While the *sp*-band Fermi surface of Ni shows a full three-dimensional bulklike topology down to the thinnest films, the *d*-band Fermi surface rearranges from a bulklike configuration in the thick films to a two-dimensional topology in the thinnest films. The reduced number of *d* holes in the thin films is explained with the rearrangement of the characteristic *K*-point lobe of the Ni Fermi surface.

DOI: 10.1103/PhysRevB.79.155404 PACS number(s): 73.61.At, 79.60.Dp

I. INTRODUCTION

At the limit of a few atomic layers of thickness, ultrathin films of magnetic materials attain properties different from the bulk in particular due to two effects. On one hand the lattice periodicity perpendicular to the film is broken, and the electronic bands may rearrange in a two-dimensional (2D) dispersion when the electrons are confined perpendicular to the film. For itinerant ferromagnets this can be expected to affect their magnetic moments and order. On the other hand the reduced film thickness leads to fewer atoms in the nearest and more distant neighbor shells, which again affects the formation of the magnetic order. Ferromagnetic transition temperatures T_C are generally reduced at low thickness due to the growing importance of magnetic fluctuations in lower dimensions.[1] The case of Ni/Cu(001) has attracted special interest for its simplicity, as Ni grows pseudomorphically on the structurally equivalent fcc Cu substrate[2] and for its spin-reorientation transition (SRT).[3] At layer thicknesses below 6–8 atomic monolayers (MLs), the magnetic easy axis is in the film plane and switches to out of plane above. The transition thickness to the out-of-plane situation depends on the adsorption of molecules and on the capping by metal overlayers[4,5] and can be as low as 5 ML in carefully prepared O/Ni/Cu(001) samples.[6] The SRT has been the subject of many studies and is understood as a subtle balance between thickness-independent volume and thickness-dependent surface and interface anisotropy energies.[5]

In the same system of Ni/Cu(001) a striking observation was made at the ultimate lower limit of 1–2 ML thickness: the electronic structure was observed to have a dispersion with respect to the momentum perpendicular to the surface, although the corresponding electrons clearly come from the 2D Ni layer.[7] The Fermi surface was even described as compatible with bulk Ni down to the lowest thickness. This angular-resolved photoemission experiment is in striking contrast with other electron spectroscopy data at the Γ point that find electronic dispersions that are compatible with a 2D structure and a transition to three-dimensional (3D) behavior between 2 and 3 ML.[8] Moreover, the analysis of *d* holes from magnetic circular dichroism experiments shows an evolution of the electronic structure with thickness that saturates only at $\approx$6 ML.[9] The 2D character is further supported by the observation of quantum well states in the unoccupied electronic structure.[10,11]

The electronic dimensionality transition happens in a thickness range well below the SRT, yet the observation is important for the magnetism as the itinerant electrons carry the magnetic moments. The electronic states develop coherently throughout the film, thus a separation into surface and interface contributions is not justified, although the concept of a separation of a surface and interface layer and the bulk has been useful for the understanding of the magnetic properties.[12] Yet the tendency to form a 2D dispersion influences the electronic anisotropy and thus also the magnetic anisotropy.[13] In this paper we aim to resolve the controversy of the conflicting observations of 3D and 2D electronic properties at the lowest film thickness (Refs. 7 and 8, respectively) by a extensive angle-resolved photoemission study. In addition, our data allow us to discuss the evolution of the *d* band that attains its bulk configuration only above 6 ML.[9]

The momentum space covered in our experiments is shown in Fig. 1. The calculated spin-polarized Fermi surface of bulk Ni is shown in two cuts of the first Brillouin zone (BZ) along with circles that mark the momentum surface of a free-electron final-state model in angular scans of photoemission. A 3D Fermi surface is manifest in the change in features with photon energy, given by the crossings of Fermi surfaces and final-state spheres, and in the match of the observed pattern with the bulk calculation. Indeed both of these criteria have been met for certain features in the work in Ref. 7. A 2D electronic structure, on the other hand, would show no variation with photon energy, except for the relative intensities of photoemission features. Furthermore, the different symmetry of the 2D BZ leads to well-assigned peaks at specific high symmetry points as observed at the Γ point in Ref. 8.

This paper is organized as follows. Sections II and III detail the experimental situation and the theoretical calculations. Section IV discusses the observed evolution of electronic energy bands with film thickness, including also the observation of magnetic order as reflected in the exchange splitting. Sections V and VI discuss the specific observations

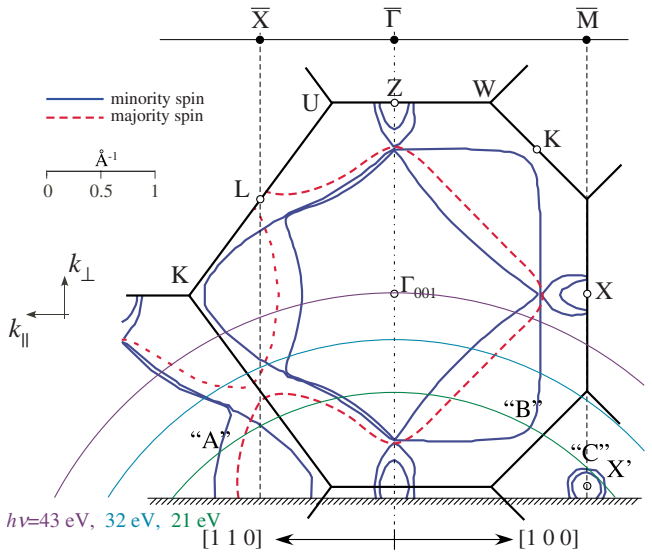

FIG. 1. (Color online) Calculated Fermi surface contours of bulk Ni in the {110} (left part) and {100} planes (right part). Majority spin *sp*-band sheets are marked by dashed lines and minority spin *sp*- and *d*-band sheets by solid lines. The repeated zone scheme shows the Brillouin zone centered at Γ_{001}. The free-electron photoemission final states as expected for emission from the (001) surface with $h\nu$=21, 32, and 43 eV are indicated by circles. The periodicity of the surface lattice is marked by the surface Brillouin zone boundaries $\bar{X}$ and $\bar{M}$.

of 2D and 3D features, respectively. These observations are discussed and conclusions are drawn in the final section.

II. EXPERIMENT

The data discussed in this paper were acquired using the COPHEE electron spectrometer.[14] It is equipped with an EA125 photoelectron analyzer (20 meV and 1° energy and angular resolution, respectively), a two-axis sample goniometer, and radiation sources of vacuum ultraviolet (vuv) light, soft x rays, and access to synchrotron vuv radiation. The Mott detectors for spin-resolved detection were not used in this study.

The mechanically polished Cu(001) substrate was cleaned by electropolishing in orthophosphoric and sulfuric acid for 2 min at 1.5 $\mathrm{mA/mm^2}$ and repeated *in situ* cycles of Ar^+ ion sputtering at 1 keV and annealing to 820 K. For related experiments on magnetized samples, the substrate was mounted in a soft iron horseshoe magnet made of ARMCO steel. The nine loops of Ta wire wound around the bottom of the horseshoe serve as an electromagnet (pulsed magnetizing field) and for heating the sample. The residual magnetization of this *in situ* system was small enough to give reliable measures on band dispersions but leads to some slight distortions of the angular mapping. The sample cleanliness was confirmed by the observation of a sharp surface state.

Ni films were deposited from a Ni rod heated by electron bombardment at 2 keV (9.4 W) in a water cooled evaporator. The vacuum pressure remained below 1×10^{-9} mbar during evaporation. The Ni flux was monitored by a quartz microbalance. The film thickness was measured by recording the intensities of Ni 3*s* and Cu 3*s* core level photoemissions using Si K_α excited x-ray photoelectron spectroscopy (XPS) for all films at the end of data taking. The inelastic mean-free path λ_i that enters the thickness calculation from the XPS intensities was calibrated by preparing one sample while observing oscillations of the reflectivity of a 3 keV beam of electrons. The reflectivity in a medium energy electron diffraction (MEED) experiment is directly related to the amount of flat (001) oriented terraces on the surface. The oscillatory behavior during evaporation shows the layer-by-layer growth and serves to measure the absolute film thickness. In this way a mean-free path of $\lambda_i=12\pm0.5$ ML at $E^m_{\mathrm{kin}}=1620$ eV was determined, which is in the upper range of the literature data.[15] The thus determined film thickness is a continuous value. Noninteger numbers correspond to partially filled layers, where a superposition of spectral features from adjacent integer layers is expected.

The Ni films were deposited at room temperature. To further reduce the roughness of the films, they were annealed to 420 K during 15 min, taking care not to exceed the temperature limit for interdiffusion.[2] This procedure always increased the sharpness of photoemission features. The crystallinity before and after evaporation was checked by low energy electron diffraction (LEED), which showed a sharp 1×1 structure on a low background in all cases. An exchange of Cu and Ni in the top layer as suggested by experimental[16] and theoretical studies[17] might be present in these samples and could add an uncertainty for the thickness determination of the thinnest films. A direct experimental signature of this effect was, however, not observed.

Angle-resolved photoemission data were acquired in two experimental situations. A first set of data as a function of film thickness was acquired using a microwave driven low-pressure He lamp.[18] The lamp was unmonochromatized and the spectrometer was set to line up the Fermi level with the photon energy $h\nu$=21.2 eV of the dominant He I_α line. The sample temperature was held at T=150 K by a flow of liquid N_2 in the cooling system of the goniometer. A second data set was acquired using synchrotron radiation delivered by the surface and interface spectroscopy (SIS) beamline at the Swiss Light Source. The photon energy was varied between 21, 32, and 43 eV. The linear polarization was in the horizontal plane of light incidence and detection of the emitted electrons. The angle-scanned data use the goniometer that turns the sample by an axis perpendicular to this plane, thus defining the polar angle of emission θ and a second axis normal to the sample surface that defines the azimuth ϕ. The light polarization is thus always *p* polarized (with respect to the sample surface). The resulting symmetry selection rules suppress emission from *ungerade* states if the azimuthal angle brings a mirror symmetry into the detection plane. In this second data set the temperature was held at T=60 K by a flow of liquid He.

Photoemission normal emission spectra excited by the He lamp are shown in Fig. 2. The evolution of the *d*-band intensity (marked as Ni d_α) near the Fermi level (binding energy E_B=0) is seen with increasing film thickness. At the same time, the Cu *d*-band peaks are reduced as the electrons from deep layers are suppressed. However, at 5.8 ML thickness of

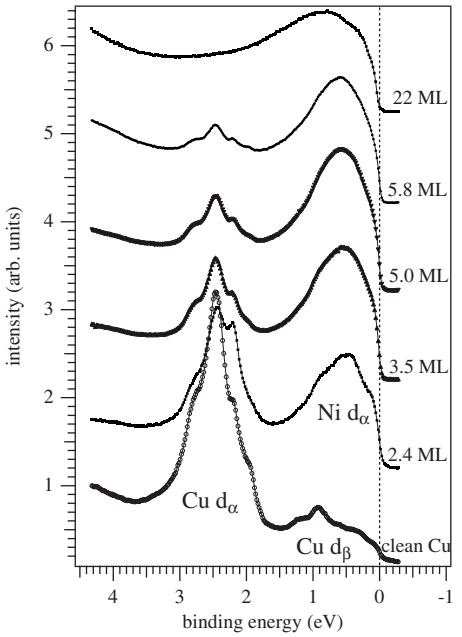

FIG. 2. Normal emission spectra of photoemission with He I radiation from nickel films on Cu(001) for various thicknesses as indicated. The data were measured with the light incident along the [100] azimuth (except for the 2.4 ML). The sample temperature was $T=150$ K (except for clean Cu, where $T=300$ K). The features and contributions from He I_α and He I_β are discussed in the text.

Ni the underlying Cu substrate peaks are still clearly visible. Since the radiation from the He lamp is not filtered by a monochromator, all features are doubly visible for He I_α ($h\nu=21.2$ eV) and He I_β ($h\nu=23.1$ eV) radiations. The Fermi level was calibrated for the dominant He I_α contribution, thus the He I_β-excited features extend to energies above the Fermi level. In Fig. 2 the features identified from He I_α are marked Cu d_α and Ni d_α, the one from He I_β is marked as Cu d_β. Only for Cu does this parasitic intensity lead to sharp discernible features at E_F, while for Ni it only gives a smooth featureless background. The binding energy of 1.9 eV that corresponds to the difference in photon energy is below the width of the d band in Ni and thus only weak features from the Ni sp band are duplicated in the vicinity of the Fermi level.

The data sets were normalized as follows to remove the strong reduction in intensity at large emission angles and with binding energy. For photoemission dispersion scans as shown in Fig. 3 each momentum-distribution curve (MDC) was first normalized by division with its mean value. Then the resulting spectra or energy distribution curves (EDCs) were again normalized by division with the mean value. This procedure enhances the visibility of bands over the whole angular and binding energy range but bears the danger of suppressing nondispersive features. The Fermi surface maps as shown in Figs. 6 and 9 were normalized by dividing each circular scan at constant polar angle by its mean value. With this normalization, the extraction of MDCs over large angular ranges is possible, as shown in Figs. 8 and 10. All features that we will discuss have been visible in the raw data. Spurious intensity due to specular reflection of UV light

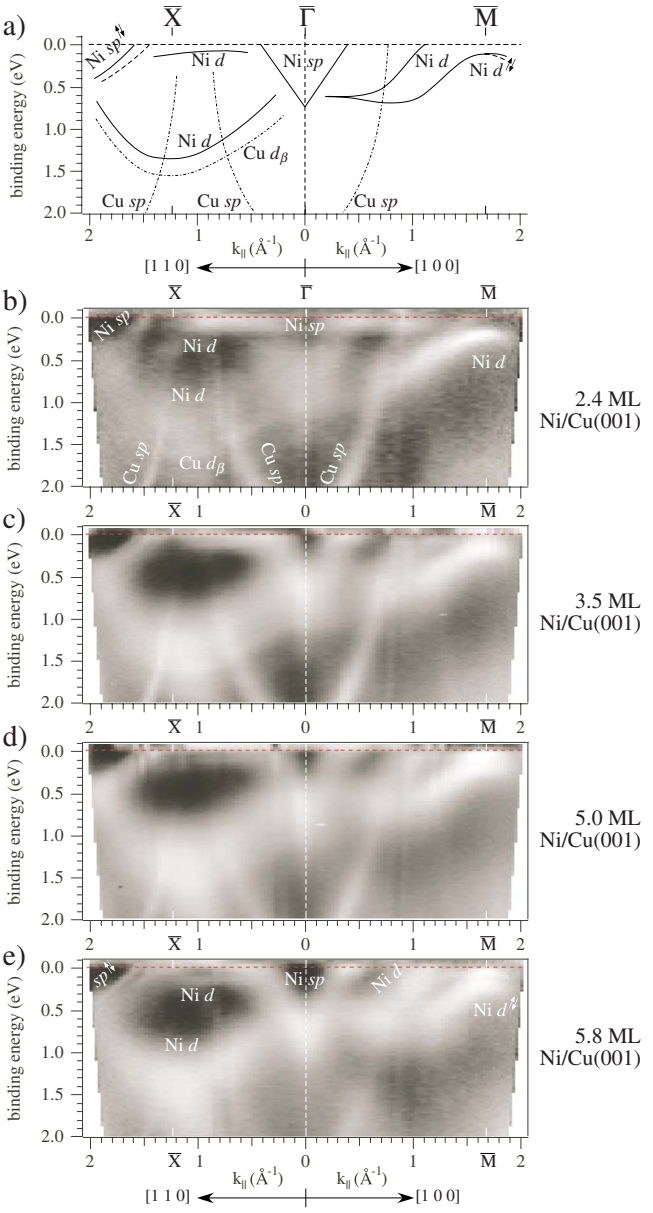

FIG. 3. (Color online) Intensity maps measured in the [110] azimuth (left part) and the [100] azimuth (right part) for various thicknesses of Ni/Cu(001) as indicated. All data were acquired using He I radiation ($h\nu=21.22$ eV) at $T=150$ K. The top panel shows a sketch of the features and their identification.

from the light source into the analyzer was removed by subtracting a given intensity from the affected spectra in the photoemission dispersion scans. In the Fermi surface maps, this procedure could not be applied and the artifact is visible as a bright ring at constant emission angle of $\theta=22.5°$.

III. CALCULATIONS

The electronic structure of the thinnest Ni films was modeled using *ab initio* calculations with the WIEN97 code.[19] A model structure of the Ni/Cu(001) films was constructed by a Cu slab of five layers in the (001) orientation and Ni films of one or two layers added on both sides of this slab with a

contracted layer distance to conserve the atomic volume of Ni.[20] The stability of this model structure was checked by calculating *ab initio* the interatomic forces that were all found to be below 1 nN. The linearized augmented plane-wave (LAPW) basis of the WIEN97 code was used to calculate projections of the resulting bands on Ni atoms and on specific angular momentum states within the atomic sphere. To mimic the collapsed exchange splitting above the Curie temperature T_C, the calculations were performed spin restricted thus forcing degeneracy between spin-up and spin-down states. This artificial procedure was found to reproduce well the band structure of paramagnetic fcc Ni in previous studies.[21]

IV. THICKNESS DEPENDENCE AND EXCHANGE SPLITTING

The evolution of the electronic structure is shown in the dispersion plots in Figs. 3(b)–3(e). At low film thickness, the features of the Cu substrate are still clearly visible. The features of the Ni bands resemble the dispersions seen in the data at high film thickness. This suggests that the electronic structure in an ultrathin Ni film is indeed similar to that in the bulk. The *sp* bands of Ni are seen on the left of the $\bar{X}$ point and in the center of the graph around the $\bar{\Gamma}$ point. At low film thickness this band is rather broad, in particular near $\bar{\Gamma}$, and then sharpens with increased thickness. The dispersion of some of the *d* bands is seen along $\bar{\Gamma}$-$\bar{X}$ as a broad feature with a band bottom at around 1.3 eV binding energy at $\bar{X}$. At low film thickness, where the features from the Cu substrate "shine through," a sharper feature is seen at slightly higher binding energy due to He I_β emission of the Cu *d* bands. The difference of photon energies between He I_α and He I_β (1.9 eV) is just slightly smaller than the difference in binding energy for the *d* bands in Ni and Cu. Sharp strongly dispersing bands across the whole binding energy range stem from Cu *sp*-band emission by He I_α radiation. Another Ni *d* band is seen dispersing along $\bar{\Gamma}$-$\bar{M}$ with an upper band apex at $\bar{M}$.

The sharpening up of the Ni *sp* band close to $\bar{\Gamma}$ is explained by the reduced broadening in momentum $k_\perp$ perpendicular to the surface with increasing film thickness. In Fig. 1 it is seen that the region around $\bar{\Gamma}$ corresponds to an *sp* Fermi surface that runs diagonally through the probed region at $h\nu$=21 eV. The effect of $k_\perp$ broadening is much more pronounced in the thin films due to smaller depth of emission. This effect of broadening is an indication of a confinement of the *sp* electrons to the Ni film; otherwise their dispersion follows closely the one of bulk Ni. Outside of $\bar{X}$ [marked "A" in Fig. 3(a)], the *sp* Fermi surface runs almost parallel to $k_\perp$ and the bands are sharp throughout the thickness range.

In contrast, the Ni *d*-band features behave quite differently. They broaden with increasing film thickness due to the appearance of an exchange splitting[22] as the Curie temperature T_C exceeds the measurement temperature that was kept constant at $T=150\pm10$ K.[23] This opening of the exchange splitting with increasing T/T_C is shown in Fig. 4(b) in spectra at the $\bar{M}$ point. The *d*-band peak broadens as the majority spin and minority spin features split apart. The width at 2.4 ML (0.15 eV) corresponds to the completely collapsed *d*-band peak width ($T>T_C=100$ K).[23]

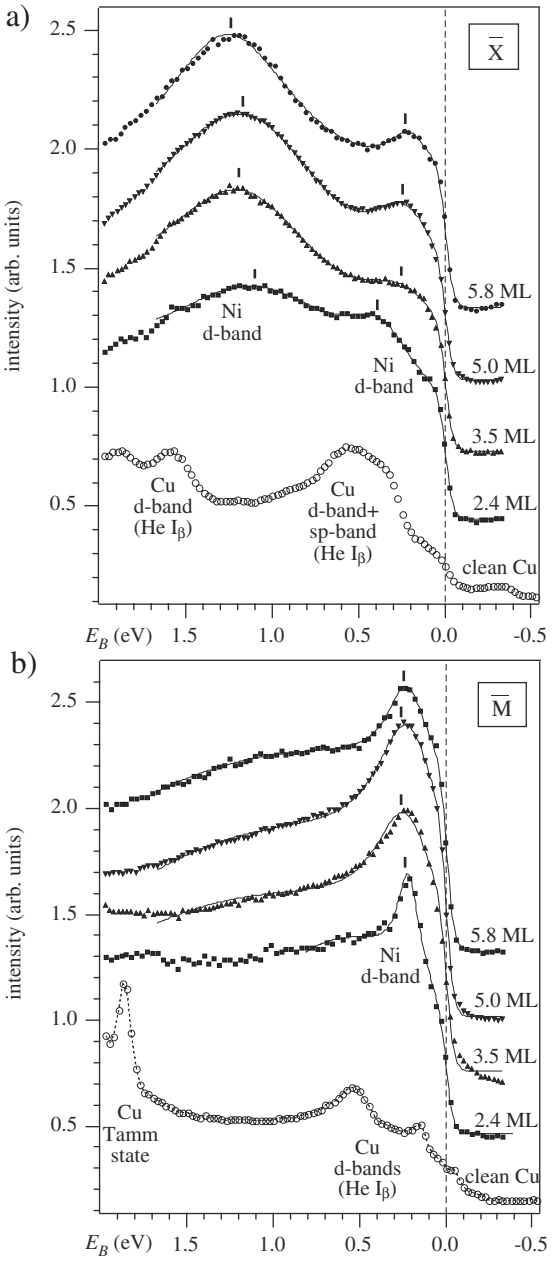

FIG. 4. Spectra for various Ni film thicknesses (a) at the $\bar{X}$ point and (b) near the $\bar{M}$ point. These spectra were extracted from the data sets shown in Fig. 3 before normalization. Fitted positions of Lorentzian peaks in the fits are marked.

V. TWO-DIMENSIONAL *d* BANDS BELOW 2 ML THICKNESS

The evolution of the occupied *d*-band binding energies at the Γ point was previously observed in Ref. 8. A distinct transition between a 2D situation at around 2 ML film thick-

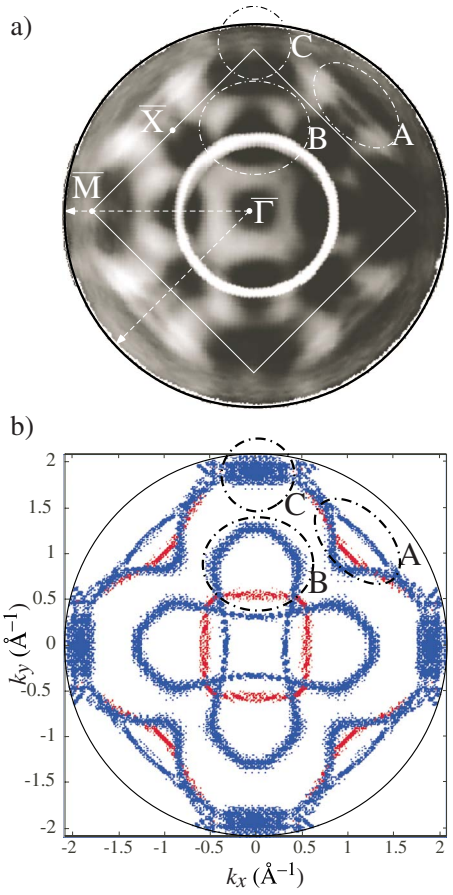

FIG. 5. (Color online) (a) Fermi surface map of a 22 ML thick film at $T=150$ K. The surface Brillouin zone is indicated along with the scan directions used in the data shown in Fig. 3. (b) Calculated cut through the Fermi surface of bulk Ni on the spherical surface scanned in (a) as shown in Fig. 1. Regions of special interest marked A–C are discussed in the text.

ness and below and a situation compatible with bulk Ni at 4 ML thickness and above was found. A similar jump of binding energy is seen in the data in Fig. 4(a) for the spectra at the $\bar{X}$ point. This point does not correspond to a high symmetry point in the 3D band structure when measured at $h\nu=21$ eV (cf. Fig. 1), but the jump in binding energy for both *d*-band features observed in these spectra leads us to inspect the Fermi surface maps of the films for features of 2D and 3D behaviors.

The limiting case of the bulk electronic structure is shown in Fig. 5. The data ($h\nu=21$ eV) are compared to a calculation of the spin-polarized bulk electronic structure of fcc Ni. The free-electron final-state model is applied with an inner potential $V_0=10.7$ eV and the Fermi surface cuts are shown in a broadening scheme corresponding to v_F. Strongly dispersing *sp* bands appear as sharp split features, while the less dispersive *d* bands are broader. A patch of intensity at $\bar{M}$ is due to the proximity of the final-state cut to the *X* point and its minority spin pocket (cf. Fig. 1). The surface Brillouin zone is indicated in Fig. 5(a) as a reference, but all features are well explained by the bulk Fermi surface of Ni.[24] They are, with labels indicated in the figure, (A) a straight section parallel to the surface Brillouin zone boundary just outside $\bar{X}$. This feature is related to the *sp* band of Ni. Feature (B) is an arc stretching out in the direction of the $\bar{M}$ point. The calculation assigns this feature to the *d*-band lobe in the direction of the *K* point of bulk Ni. Feature (C) is a patch of intensity right at the $\bar{M}$ point. A square feature around $\bar{\Gamma}$ is due to the Ni *sp* band as discussed above. All these features appear also as bands crossing the Fermi level in Fig. 3. The prominent ringlike feature at $k_{\|}=0.8$ Å^{-1} is an artifact due to direct reflection of UV light into the analyzer at $\theta=22.5°$.

The evolution of the Fermi surface with reduced film thickness can be traced in Figs. 6(a)–6(e). The data from the 5.8 ML film strongly resemble the bulk data except for a slightly lower visibility of the *d*-band arc [feature (B)]. Going to 5 and 3.5 ML thicknesses, the features evolve smoothly. The *sp*-band square around $\bar{\Gamma}$ broadens, as discussed above. The *sp*-band segment outside of the $\bar{X}$ point [feature (A)] remains sharp but the exchange splitting is reduced. The *d*-band arc [feature (B)] is further reduced in intensity and no longer observed at 3.5 ML thickness. The patch of intensity at the $\bar{M}$ point [feature (C)] gains in intensity and a new structure develops around it.

In the Fermi surface map at 2.4 ML thickness most features have completely changed. Unchanged are only the square around $\bar{\Gamma}$ that is now very broad and the *sp*-band segment outside of $\bar{X}$, now without exchange splitting as $T>T_C$. Along the line $\bar{\Gamma}$-$\bar{X}$ a bar of intensity is visible that is already slightly seen at 3.5 ML thickness. The *d*-band arc (region B) on the other hand has completely disappeared. So has the patch of intensity at $\bar{M}$, which is replaced by an oval feature circling around $\bar{M}$. Outside of the bright artifact ring, at $k_{\|}=0.8$ Å^{-1} a new straight segment parallel to the Brillouin zone boundary has appeared.

The band structures and Fermi surface maps resulting from our slab calculations for 1 and 2 ML of Ni on Cu(001) are shown in Fig. 7. The regions of the surface-projected density of states on the Cu substrate are seen as an artifact set of five steep bands from the *sp* electrons of each Cu layer. The ultrathin Ni films on the other hand are well represented by the calculations. They match the results of earlier calculations[25] except for the absence of exchange splitting in our paramagnetic calculation. In the band structure plot, a projection on Ni atoms is shown as circles that highlight the corresponding bands (fat-band representation). In the Fermi surface maps, the gray levels correspond to the distance of the electronic levels from the Fermi level. Weakly dispersive bands close to E_F lead to broad features, while steep bands such as the *sp* bands of both Cu and Ni give sharp lines.

The characteristic features of the slab calculations are visible in the Fermi surface maps in Fig. 7: (i) a ring-shaped hole pocket is seen around the $\bar{M}$ point; (ii) a broad streak due to a flat band close to E_F is seen along the line $\bar{\Gamma}$-$\bar{X}$; and (iii) slightly curved segments of the *sp*-band derived Fermi surface are seen parallel to the Brillouin zone boundary near $\bar{X}$ in the calculation of the 1 ML film. In the 2 ML film these segments are still visible if all bands are represented but

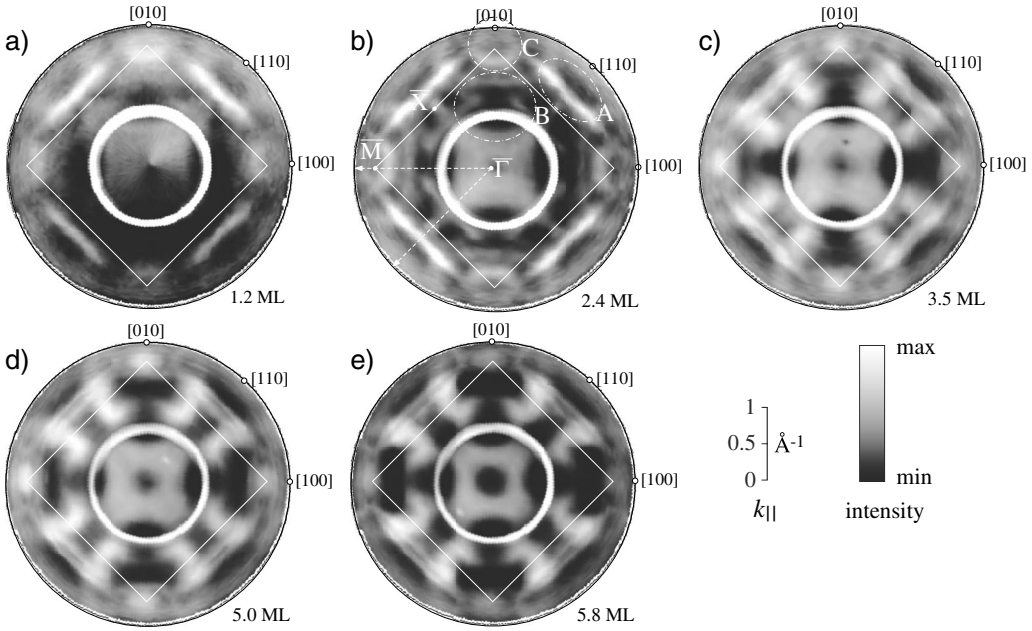

FIG. 6. Fermi surface maps of Ni films of various thicknesses on Cu(001) measured with He I radiation ($h\nu$=21.22 eV) at T=150 K [except (a), where T=300 K]. The film thickness is indicated in ML and the surface Brillouin zone is marked. The normalization procedure for the linear gray scale is described in Sec. II. A bright ring at $k_{\|}$=0.8 Å^{-1} is an artifact due to reflection of UV light into the analyzer.

become hardly discernible when the projections are applied. The symmetry of the maps obviously matches the lateral periodicity of the model unit cell, i.e., the surface lattice; thus all features appear multiple times within the radius of the photoemission horizon at $k_{\|}$=2.04 Å^{-1} (white circle).

By comparison of the experimental Fermi surface maps to the calculations shown in Fig. 7 we arrive at the following assignment of the features of Fig. 6(b). The square around $\bar{\Gamma}$ and the segment outside of $\bar{X}$ are due to *sp*-band Fermi surface cuts. The other features are specific to a two-dimensional electronic structure. The bar of intensity along $\bar{\Gamma}$-$\bar{X}$ is due to a flat band close to E_F. A high intensity close to E_F is also visible in the dispersion maps in Fig. 3. An unambiguous assignment is, however, only possible in the momentum-distribution maps in Fig. 6 that do not suffer from the Fermi cutoff and artifacts due to normalization of the intensities along the energy axis. In bulk Ni a *d* band just above E_F is expected in this region. Thus the feature is assigned to a Ni *d* band that becomes just slightly occupied due to a shift in its binding energy. The ring feature around $\bar{M}$ is also reproduced in the calculations although the Fermi wave vectors do not match precisely. This feature is discernible in Fig. 3 as a band dispersing parallel to the fully occupied *d* band at $\bar{M}$. The momentum structures of the two features are readily visible in the Fermi surface maps (Fig. 6). The calculations show that these two features are due to Ni *d* bands. The last feature to be assigned is the straight segment parallel to the Brillouin zone boundary at $k_{\|} \simeq 1$ Å^{-1}. This feature is seen in the calculation for a 1 ML film as a *sp*-like segment. It is parallel to the *sp*-band segment "C" outside the $\bar{X}$ point and the position is almost mirror symmetric with respect to $\bar{X}$. Thus we arrive at assigning this feature as an umklapp of the *sp* band. The whole Fermi surface map at 2.4 ML thickness is much more symmetric with respect to the surface Brillouin zone than the data from thicker films that match the expected bulk band structure.

The calculated Fermi surface maps of Fig. 7 are represented with various projections of the total spectral weight on specific atoms and angular momentum states. The projections are provided by the augmented plane-wave basis of the WIEN97 code and correspond to the wave functions inside the respective atomic spheres. For the 1 ML calculation in Fig. 7(a) the total spectral weight (all) is shown along with projections on all angular momenta of the Ni atom ($\mathrm{Ni}_{\mathrm{tot}}$), on only the *d* orbitals of the Ni atom (Ni *d*), and the *p* orbitals of the Ni atom (Ni *p*). In Fig. 7(b) for the two layer films, the interface and surface Ni atom, are distinguished as Ni_I ($\mathrm{Ni}_{I\,\mathrm{tot}}$) and Ni_S ($\mathrm{Ni}_{S\,\mathrm{tot}}$), respectively. The sum of these projections on Ni_S and Ni_I is shown as ($\mathrm{Ni}_{S\,\mathrm{tot}}$+$\mathrm{Ni}_{I\,\mathrm{tot}}$). The ring-like feature around the $\bar{X}$ point is only visible in projections in *d* orbitals for all Ni atoms. It is thus assigned to a two-dimensional *d*-band feature. The same holds for the streak of spectral weight along the $\bar{\Gamma}$-$\bar{X}$ line, although it is only visible for the surface atom (Ni_S in the 2 ML film). In the *p*-orbital projection, a curved line feature close to the $\bar{X}$ point is visible in the calculation of the 1 ML thick film. This feature corresponds to the *sp* band. The two-dimensional calculations show it repeatedly in the central and neighboring Brillouin zones of the repeated zone scheme.

Extracting the momentum-distribution curves along $\bar{\Gamma}$-$\bar{X}$ and $\bar{\Gamma}$-$\bar{M}$ from Fig. 6, we can analyze these features in more detail. This is shown in Fig. 8. From the bottom to the top the momentum curves from 1.2 to 22 ML thickness are shown. In the leftmost part the *sp* band outside $\bar{X}$ is seen with an increasing exchange splitting. The artificial ring due to reflected light at $k_{\|}$=0.8 Å^{-1} is shaded. Inside this ring, around $\bar{\Gamma}$ the square *sp*-band Fermi surface is seen that sharpens up

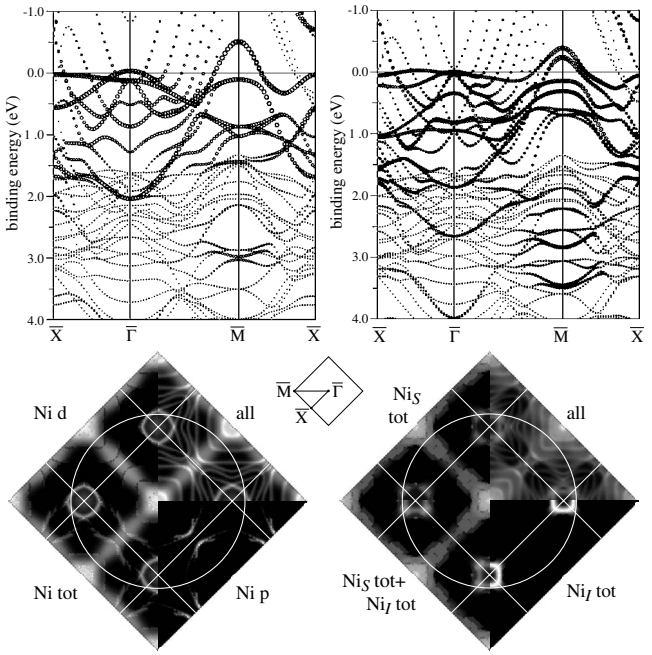

a) 1 ML Ni/5 ML Cu/1 ML Ni b) 2 ML Ni/5 ML Cu/2 ML Ni

FIG. 7. Calculated band structures and Fermi surfaces of (a) one layer Ni/Cu(001) and (b) two layers Ni/Cu(001) using the WIEN97 software (Ref. 19). In the band structure representations bands localized in the Ni layers are highlighted by circles. In the Fermi surface maps the borders of the Brillouin zone and the horizon of the He I excited photoemission experiment ($k_{\|}$=2.04 Å^{-1}) are indicated by white lines. The projections on specific atoms and orbitals are described in the text.

at large film thickness. Around the $\bar{M}$ point the change in the features is more dramatic. At low film thickness two sharp peaks are seen inside of $\bar{M}$. Gradually the first peak at $k_{\|} \simeq 1.3$ Å^{-1} moves to lower $k_{\|}$ and broadens slightly to become part of the *d*-band arc ("B"). The second peak at $k_{\|} \simeq 1.6$ Å^{-1} abruptly disappears above 2.4 ML thickness and the new broad peak due to the patch of intensity at $\bar{M}$ develops.

It should be noted that in our data the transition *d*-band structure appears above 2.4 ML as the film at this thickness still shows the features that are assigned to the two-dimensional case. In Ref. 8, however, the transition is found between 2 and 4 ML thicknesses. We think that our data from the 2.4 ML thick film are dominated by the distinct features from the 2 ML thick parts of the sample, while the 3 ML thick islands that give the features of a more 3D-like electronic structure are already slightly visible in the data. Thus we assign the transition from two- to three-dimensions at 2 ML, noting that the *d*-band structure evolves further at higher thickness.

VI. THREE-DIMENSIONAL *sp* BANDS AT ALL THICKNESSES

Sections IV and V have listed several observations of electronic states at 1–2 ML Ni thickness that are compatible with a complete 2D confinement of the itinerant states. However, a previous Fermi surface study[7] has given evidence of a 3D movement of the electrons, both through the agreement with calculations of the bulk electronic structure of Ni and through the observation of an evolution of the Fermi surface with photon energy and thus with the full momentum of the electrons. We will now inspect our data for aspects of the bulk electronic structure of Ni at low film thickness.

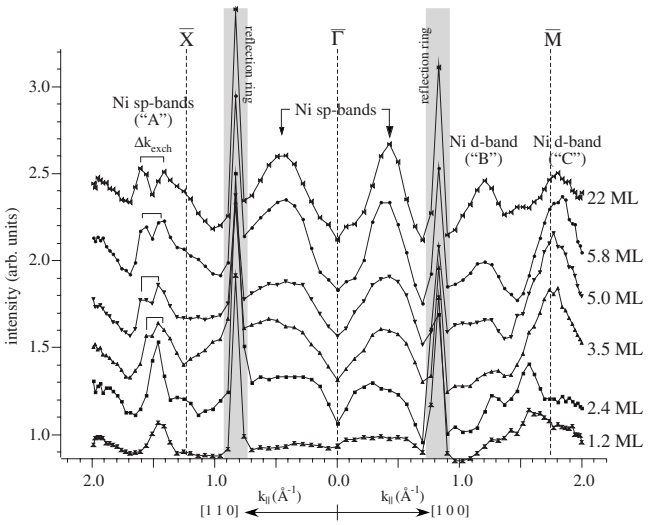

FIG. 8. Fermi edge momentum-distribution curves from Ni/Cu(001) between 1.2 and 22 ML thicknesses. The data were extracted from the maps shown in Fig. 6 making use of the normalization to remove the strong reduction in intensity a large $k_{\|}$.

A close inspection of Fig. 8 shows that two features remain at a constant $k_{\|}$ location with thickness, namely, the peak outside of $\bar{X}$ at $k_{\|}$=1.46 Å^{-1} and the *sp*-band peaks close to $\bar{\Gamma}$ at $k_{\|}$=0.4–0.5 Å^{-1}. The former splits up at high film thickness due to the opening of an exchange splitting, and the latter sharpen from very broad features at 2.4 ML thickness to well-defined features in the thick films. The positions of these features agree well with the bulk Ni calculations within a free-electron final-state model (Fig. 5), both in the position along the high symmetry direction and in the shape of the feature in the Fermi surface map.

Measurements at varying photon energies and thus varying cuts in the three-dimensional momentum space are shown in Fig. 9. Data for two films of 2 and 5 ML thicknesses are shown as well as calculations for bulk Ni in the free-electron-final-state model. These data have been acquired at a lower temperature of T=60 K and using linearly *p*-polarized light. At and in the vicinity of crystal mirror planes the selection rules suppress intensity from initial states that are ungerade with respect to that plane. This concerns the $\bar{\Gamma}$-$\bar{X}$ (100)-plane and $\bar{\Gamma}$-$\bar{M}$ (110)-plane lines. Incidentally this suppresses the *d*-band ring feature around $\bar{M}$. The *sp* electrons are *gerade* with respect to the mirror planes and their dispersion can be readily traced.

The Fermi surface calculations shown on the left side of Fig. 9 agree well with the data from 5 ML Ni/Cu(001) as expected because at 5 ML thickness the electronic structure is essentially developed as in bulk Ni. The data from the 2

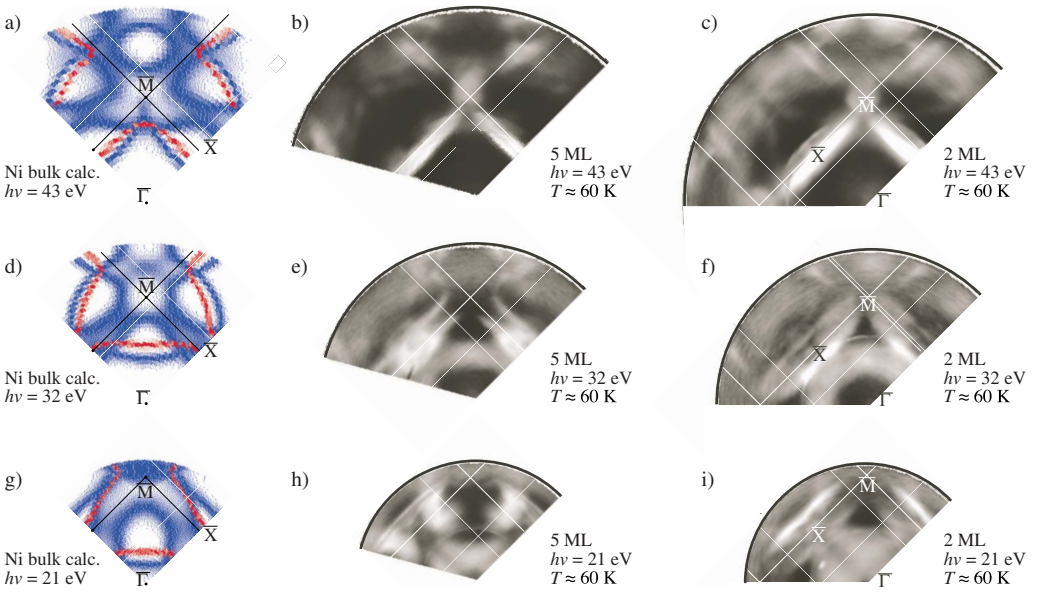

FIG. 9. (Color online) Fermi surface maps of Ni films of 5 and 2 ML thicknesses excited with *p*-polarized radiation of $h\nu$=43 eV (top), $h\nu$=32 eV (middle), and $h\nu$=21 eV (bottom). The left part shows calculated Fermi surface cuts of bulk Ni according to a free-electron final-state model at the corresponding photon energies.

ML thick film show again a general trend to be more compatible with the 2D symmetry as represented by the surface Brillouin zone. The splitting of the *sp* bands is collapsed as the measurement temperature is very close to the film's T_C. The measurements can thus be compared to the spin-restricted calculations shown in Fig. 7.

The almost straight *sp*-band Fermi surface segment in the Γ-*W*-*K* plane connecting the *X*-point pockets (cf. Fig. 1) can now be traced by following the peak positions in the momentum-distribution curves. For the upper three curves in Fig. 10, representing the 5 ML thick film, this is readily done, as they are the only intense features besides the peaks at $\bar{M}$. In the 2 ML thick film, the peak is less easily traced, as the feature is much broadened, but the same evolution of the peak position is found, going from $h\nu$=21 eV to $h\nu$ =43 eV. Thus the *sp*-band feature is found to be dispersive with full 3D momentum in a fashion that is compatible with the Fermi surface of bulk Ni.

VII. CONCLUSION

The electronic structure of ultrathin films of Ni on Cu(001) has indeed close resemblance to that of bulk Ni, down to low film thicknesses of 2.4 ML. This is evident from the band dispersion maps (Fig. 3). A more detailed view is provided by angular maps and thus by Fermi surface cuts both as a function of film thickness and at varying photon energies. It is found that all *d*-band features show a qualitative transition at a film thickness between 2 and 4 ML. This transition leads to a jump both in binding energies and in the topology of the Fermi surface. The data from a 2.4 ML thick film show all *d*-band features compatible with the 2D slab calculations of Ni/Cu(001) films. The *d*-band features at higher film thickness between 3 and 6 ML show a gradual evolution to a situation that is fully compatible with bulk Ni.

The *sp*-band Fermi surface is found fully developed at the lowest measured film thickness of 1.2 ML. Its full momentum space structure is found compatible with that of bulk Ni. A substantial broadening is found in those sections of the

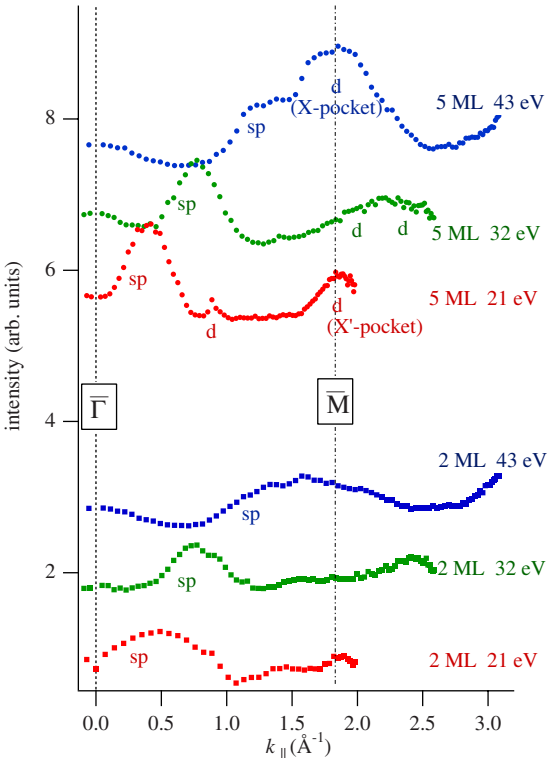

FIG. 10. (Color online) Fermi edge momentum-distribution curves form Ni/Cu(001) as extracted from the data in Fig. 9. The three curves at the top are from 5 ML thick films with different photon energies. The three curves at the bottom are from 2 ML thick films.

Fermi surface, where a $k_\perp$ uncertainty can smear out the features. This broadening is gradually removed as the film thickness is increased. Because the varying Curie temperature T_C of the films corresponds to an effectively varying T/T_C at the fixed measurement temperature $T=150$ K, the effect of the collapse of the exchange splitting is observed.

The difference between the behavior of *sp*-band electrons and *d* levels may be sought in the degree of localization of the states. Both *d* and *sp* electrons are itinerant states, but the *sp*-band wave functions are much more extended and overlap more strongly between neighboring atoms, as is evident in the large bandwidth. The *d* bands are more localized leading to a less dispersive band. In the transition metals, the *sp* bands and the *d* bands hybridize only slightly, the steep *sp* band crosses the *d*-band complex with only few avoided crossings, and the character remains always clearly defined. Indeed, despite of almost the same exchange splitting, the *d* bands carry almost all of the magnetic moment in Ni, while the *sp* bands provide the environment for a ferromagnetic coupling. In the Ni/Cu(001) films, the *d* bands hybridize little with the Cu substrate and a bulklike electronic structure is only established when most of the Ni atoms are in an environment with 12 nearest Ni neighbors as in the bulk.

Also, the *sp* electrons do not form completely hybridized states with the Cu bands, as seen in Fig. 3(b). The Ni *sp* bands and the Cu *sp* bands are seen as separate features. The binding energies of the observed Ni *sp* bands completely agree with those in bulk Ni, as the electrons move in the potential energy landscape of Ni atoms. This confinement is also evident from the broadening of the features at low film thickness that shows the reduced emission depth, leading to a smearing of the momentum $k_\perp$. The coupling of the strongly delocalized *sp*-band electrons to the Cu substrate is, however, strong enough that they sense the periodicity of the underlying lattice and develop wave functions that follow the three-dimensional symmetry of the fcc structure.

For the *d* bands the dimensionality transition at 2–3 ML is followed by a continuous evolution of the number of *d* holes.[9] Depth resolved studies have identified the evolution of *d* holes in particular with changes in the *d* configuration of Ni surface atoms,[12] which is confirmed by a recent layer-resolved analysis of the electronic structure of Ni/Cu(001) thin films.[26] In our data, the change in metric for the *d* bands when going from a two-dimensional (2D) to a 3D situation does not allow the comparison of the Fermi surface volumina and thus of the number of *d* holes in a quantitative way. In three dimensions the data at a fixed photon energy probe only specific cuts in momentum space and the full volume cannot be determined. Still, we can attempt to locate the evolution in the momentum space covered in this experiment. We can distinguish two sheets of the *d*-band Fermi surface that are visible in our cut at $h\nu=21$ eV. In the data at 2.4 ML thickness they show up as the circle around the $\bar{M}$ point and the streak of intensity along $\bar{\Gamma}$-$\bar{X}$. The former evolves into an unstructured patch of intensity at the $\bar{M}$ point that is identified as a slightly touching cut through the *X*-point pocket of bulk Ni (see Fig. 1 and Ref. 24). Seen from our data, its volume thus decreases, contrary to the expectation that the number of *d* holes should increase. This feature shows no further evolution with increasing film thickness. The latter feature along $\bar{\Gamma}$-$\bar{X}$ shows a more drastic change at the dimensionality crossover. The streak along $\bar{\Gamma}$-$\bar{X}$ in the Fermi surface maps disappears gradually and is no longer visible at 5 ML thickness. At the same time the characteristic *d*-band loop that stretches to the $\bar{M}$ point in the thick film (Fig. 5) becomes gradually visible and evolves into a well-defined feature only at 5.8 ML thickness. This change in the Fermi surface volume corresponds indeed to an increase in the number of *d* holes with film thickness as this feature corresponds to the distinct *d*-band lobe toward the *K* point in bulk Ni. The fact that some intensity remains visible at 3.5 ML thickness and above is a signature of the gradual evolution of the *d* band to the bulk situation in this thickness range.

The abrupt topological transition from the 2D to the 3D dispersion of the *d* bands is in a thickness range much below the spin-reorientation transition (SRT). The behavior of the *d* electrons, which is strongly affected by the nearest-neighbor shell, can give important hints on its contribution to the magnetic anisotropy. We conclude that the surface layer of Ni(001), deprived of four of its nearest neighbors, has the tendency to form a 2D dispersion. In the 2 ML thin film and below this leads to a fully developed 2D confinement. We conclude that the electronic structure of ultrathin films of Ni on Cu(001) below 2 ML thickness is neither bulklike as suggested by the bulklike Fermi surface features observed by Mankey *et al.*[7] nor two dimensions as derived from the *d*-band features at Γ by Pampuch *et al.*[8] Rather we have to distinguish between *sp*-band features that show indeed a Fermi surface similar to that in the bulk of Ni, except for the smearing due to confinement in the film, and the *d* electrons that show a transition from a two-dimensional situation at 2 ML film thickness and below and a gradual development of the three-dimensional structure at 3–6 ML thickness.

ACKNOWLEDGMENTS

We wish to thank the team of the machine shop of the Physics Institute of the University of Zurich for skillful mechanical work that allowed the construction of the COPHEE spectrometer. Indispensable technical assistance was given by W. Deichmann, M. Klöckner, and F. Dubi. Parts of this experiment were performed at the Swiss Light Source with the help of L. Patthey, M. Shi, and J. Krempasky. We are indebted to F. Baumberger and R. Fasel for use of their data analysis software and to the Swiss National Science Foundation for supporting this project.

*Present address: Department of Chemistry, University of Minnesota, 207 Pleasant St. SE, Minneapolis, Minnesota 55455, USA.
†Present address: Swiss Nanoscience Institute, University of Basel, Klingelbergstrasse 82, 4056 Basel, Switzerland.

[1] P. Poulopoulos and K. Baberschke, J. Phys.: Condens. Matter **11**, 9495 (1999).
[2] J. Shen, J. Giergiel, and J. Kirschner, Phys. Rev. B **52**, 8454 (1995).
[3] B. Schulz, R. Schwarzwald, and K. Baberschke, Surf. Sci. **307-309**, 1102 (1994).
[4] R. Vollmer, T. Gutjahr-Löser, J. Kirschner, S. van Dijken, and B. Poelsema, Phys. Rev. B **60**, 6277 (1999).
[5] S. van Dijken, R. Vollmer, B. Poelsema, and J. Kirschner, J. Magn. Magn. Mater. **210**, 316 (2000).
[6] J. Linder, P. Poulopoulos, R. Nunthel, E. Kosubek, H. Wende, and K. Baberschke, Surf. Sci. **523**, L65 (2003).
[7] G. J. Mankey, K. Subramanian, R. L. Stockbauer, and R. L. Kurtz, Phys. Rev. Lett. **78**, 1146 (1997).
[8] C. Pampuch, O. Rader, R. Kläsges, and C. Carbone, Phys. Rev. B **63**, 153409 (2001).
[9] P. Srivastava, N. Haack, H. Wende, R. Chauvistre, and K. Baberschke, Phys. Rev. B **56**, R4398 (1997).
[10] F. Himpsel and O. Rader, Appl. Phys. Lett. **67**, 1151 (1995).
[11] O. Karis *et al.*, Phys. Rev. B **63**, 113401 (2001).
[12] K. Amemiya, E. Sakai, D. Matsumura, H. Abe, and T. Ohta, Phys. Rev. B **72**, 201404(R) (2005).
[13] J. Hong, R. Q. Wu, J. Lindner, E. Kosubek, and K. Baberschke, Phys. Rev. Lett. **92**, 147202 (2004).
[14] M. Hoesch, T. Greber, V. N. Petrov, M. Muntwiler, M. Hengsberger, W. Auwärter, and J. Osterwalder, J. Electron Spectrosc. Relat. Phenom. **124**, 263 (2002).
[15] M. Seah and W. Dench, Surf. Interface Anal. **1**, 2 (1979).
[16] T. C. Q. Noakes, P. Bailey, and G. van der Laan, Phys. Rev. B **67**, 153401 (2003).
[17] L. V. Pourovskii, N. V. Skorodumova, Y. K. Vekilov, B. Johansson, and I. A. Abrikosov, Surf. Sci. **439**, 111 (1999).
[18] P. Baltzer, L. Karlsson, M. Lundquist, and B. Wannberg, Rev. Sci. Instrum. **64**, 2179 (1993).
[19] P. Blaha, K. Schwarz, and J. Luitz, *Wien 97, A Full Potential Linearized Augmented Plane Wave Package for Calculating Crystal Properties* (Technische Universität Wien, Austria, 1999).
[20] W. Platow, U. Bovensiepen, P. Poulopoulos, M. Farle, K. Baberschke, L. Hammer, S. Walter, S. Müller, and K. Heinz, Phys. Rev. B **59**, 12641 (1999).
[21] P. Aebi, T. J. Kreutz, J. Osterwalder, R. Fasel, P. Schwaller, and L. Schlapbach, Phys. Rev. Lett. **76**, 1150 (1996).
[22] T. J. Kreutz, T. Greber, P. Aebi, and J. Osterwalder, Phys. Rev. B **58**, 1300 (1998).
[23] U. Bovensiepen, P. Poulopoulos, M. Farle, and K. Baberschke, Surf. Sci. **402-404**, 396 (1998).
[24] Y. Miura, K. Shimada, M. Hoesch, M. Higashiguchi, N. Tobita, X. Cui, Y. Aiura, H. Namatame, and M. Taniguchi, J. Magn. Magn. Mater. **310**, 1082 (2006).
[25] X.-Y. Zhu, J. Hermanson, F. J. Arlinghaus, J. G. Gay, R. Richter, and J. R. Smith, Phys. Rev. B **29**, 4426 (1984).
[26] F. Matsui, T. Matsushita, Y. Kato, M. Hashimoto, K. Inaji, F. Z. Guo, and H. Daimon, Phys. Rev. Lett. **100**, 207201 (2008).